Reprinted from

MATERIALS SCIENCE & ENGINEERING A

Materials Science and Engineering A229 (1997) 23–41

Shear localization and recrystallization in high-strain, high-strain-rate deformation of tantalum

V.F. Nesterenko [b], M.A. Meyers [a,b,*], J.C. LaSalvia [a,b], M.P. Bondar [c], Y.J. Chen [b], Y.L. Lukyanov [c]

[a] *Institute for Mechanics and Materials, Department of Applied Mechanics and Engineering Sciences, San Diego, La Jolla, CA 92093-0411, USA*
[b] *Department of Applied Mechanics and Engineering Sciences, University of California, San Diego, La Jolla, CA 92093-0411, USA*
[c] *Lavrentyev Institute of Hydrodynamics, Russian Academy of Sciences, Novosibirsk, 630090, Russia*

Received 24 July 1995; received in revised form 27 November 1996

ELSEVIER

MATERIALS SCIENCE AND ENGINEERING A

The journal provides an international medium for the publication of theoretical and experimental studies and reviews of the properties and behavior of a wide range of materials, related both to their structure and to their engineering application. The varied topics comprising materials science and engineering are viewed as appropriate for publication: these include, but are not limited to, the properties and structure of crystalline and non-crystalline metals and ceramics, polymers and composite materials.

Types of contributions
Original research work not already published; plenary lectures and/or individual papers given at conferences; reviews of specialized topics within the scope of the journal; engineering studies; letters to the editor.

Subscription Information 1997
Volumes 222–238, each volume containing 2 issues, are scheduled for publication. Prices are available from the publishers upon request. Subscriptions are accepted on a pre-paid basis only. Issues are sent by SAL (Surface Air Lifted) mail wherever this service is available. Airmail rates are available upon request.

Orders, claims, and product enquiries: please contact the Customer Support Department at the Regional Sales Office nearest you:

New York
Elsevier Science
P.O. Box 945
New York, NY 10159-0945, USA
Tel.: (+1) 212-633-3730
[Toll free number for North American customers: 1-888-4ES-INFO (437-4636)]
Fax: (+1) 212-633-3680
E-mail: usinfo-f@elsevier.com

Amsterdam
Elsevier Science
P.O. Box 211
1000 AE Amsterdam
The Netherlands
Tel.: (+31) 20-4853757
Fax: (+31) 20-4853432
E-mail: nlinfo-f@elsevier.nl

Tokyo
Elsevier Science
9–15 Higashi-Azabu 1-chome
Minato-ku, Tokyo 106
Japan
Tel.: (+81) 3-5561-5033
Fax: (+81) 3-5561-5047
E-mail: kyf04035@niftyserve.or.ij

Singapore
Elsevier Science
No. 1 Temasek Avenue
#17-01 Millenia Tower
Singapore 039192
Tel.: (65) 434-3727
Fax: (+65) 337-2230
E-mail: asiainfo@elsevier.com.sg

Abstracting and/or Indexing Services
American Ceramic Society; Cambridge Scientific Abstracts; Chemical Abstracts; Current Contents; Engineering Index; FIZ Karlsruhe; Fluid Abstracts; Fluidex; Glass Technology Abstracts; Inspec/Physics Abstracts; Metals Abstracts; Pascal (Centre National de la Recherche Scientifique); Physikalische Berichte; Research Alert™; Science Citation Index.

ELSEVIER

Materials Science and Engineering A229 (1997) 23–41

MATERIALS SCIENCE & ENGINEERING A

Shear localization and recrystallization in high-strain, high-strain-rate deformation of tantalum

V.F. Nesterenko [b], M.A. Meyers [a,b,*], J.C. LaSalvia [a,b], M.P. Bondar [c], Y.J. Chen [b], Y.L. Lukyanov [c]

[a] *Institute for Mechanics and Materials, Department of Applied Mechanics and Engineering Sciences, San Diego, La Jolla, CA 92093-0411, USA*
[b] *Department of Applied Mechanics and Engineering Sciences, University of California, San Diego, La Jolla, CA 92093-0411, USA*
[c] *Lavrentyev Institute of Hydrodynamics, Russian Academy of Sciences, Novosibirsk, 630090, Russia*

Received 24 July 1995; received in revised form 27 November 1996

Abstract

Tantalum was subjected to high plastic strains (global effective strains between 0 and 3) at high strain rates ($> 10^4\ s^{-1}$) in an axisymmetric plane strain configuration. Tubular specimens, embedded in thick-walled cylinders made of copper, were collapsed quasi-uniformly by explosively-generated energy; this was performed by placing the explosive charge co-axially with the thick-walled cylinder. The high strains achieved generated temperatures which produced significant microstructural change in the material; these strains and temperatures were computed as a function of radial distance from the cylinder axis. The microstructural features observed were: (i) dislocations and elongated dislocation cells ($\epsilon_{eff} < 1$, $T < 600$ K); (ii) subgrains ($1 < \epsilon_{eff} < 2$, 600 K $< T <$ 800 K); (iii) dynamically recrystallized micrograins ($2 < \epsilon_{eff} < 2.5$, 800 K $< T <$ 900 K); and (iv) post-deformation recrystallized grains ($\epsilon_{eff} > 2.5$, $T > 1000$ K). Whereas the post-deformation (static) recrystallization takes place by a migrational mechanism, dynamic recrystallization is the result of the gradual rotation of subgrains coupled with dislocation annihilation. A simple analysis shows that the statically recrystallized grain sizes observed are consistent with predicted values using conventional grain-growth kinetics. The same analysis shows that the deformation time is not sufficient to generate grains of a size compatible with observation (0.1–0.3 μm). A mechanism describing the evolution of the microstructure leading from elongated dislocation cells, to subgrains, and to micrograins is proposed. Grain-scale localization produced by anisotropic plastic flow and localized recovery and recrystallization was observed at the higher plastic strains ($\epsilon_{eff} > 1$). Residual tensile 'hoop' stresses are generated near the central hole region upon unloading; this resulted in ductile fracturing along shear localization bands. © 1997 Elsevier Science S.A.

Keywords: Plastic strains; Recrystallization; Tantalum

1. Introduction

The combined effects of high strain rate and high plastic strain on metals can generate a broad range of microstructural changes: work hardening, dynamic recovery, dynamic recrystallization, phase transformations, and even melting. These effects are important in many applications (e.g. metal forming, machining, terminal ballistic effects, etc.) and can lead to localized softening and shear-band formation. Shear bands are a very important deformation mechanism at high strain rates, and the ability to predict their occurrence and frequency requires a detailed knowledge of the constitutive response of the material, as well as of the microstructural softening processes (recovery, recrystallization, phase changes, precipitate dissolution, etc.) and of the mechanics of localization evolution. Tantalum and tantalum-tungsten alloys are excellent materials for chemical-energy penetrators (shaped charges and explosively-forged projectiles (EFP)) because of their high density ($\rho \sim 16.7 \times 10^3$ kg m^{-3}) and considerable ductility and strength. In explosively forged projectiles the effective plastic strains can reach levels of several hundred percent [1,2], whereas in shaped charges they can be even higher. Characterization and analysis of the microstructural changes under these extreme conditions has been carried out by Murr

* Corresponding author.

PII S0921-5093(96)10847-9

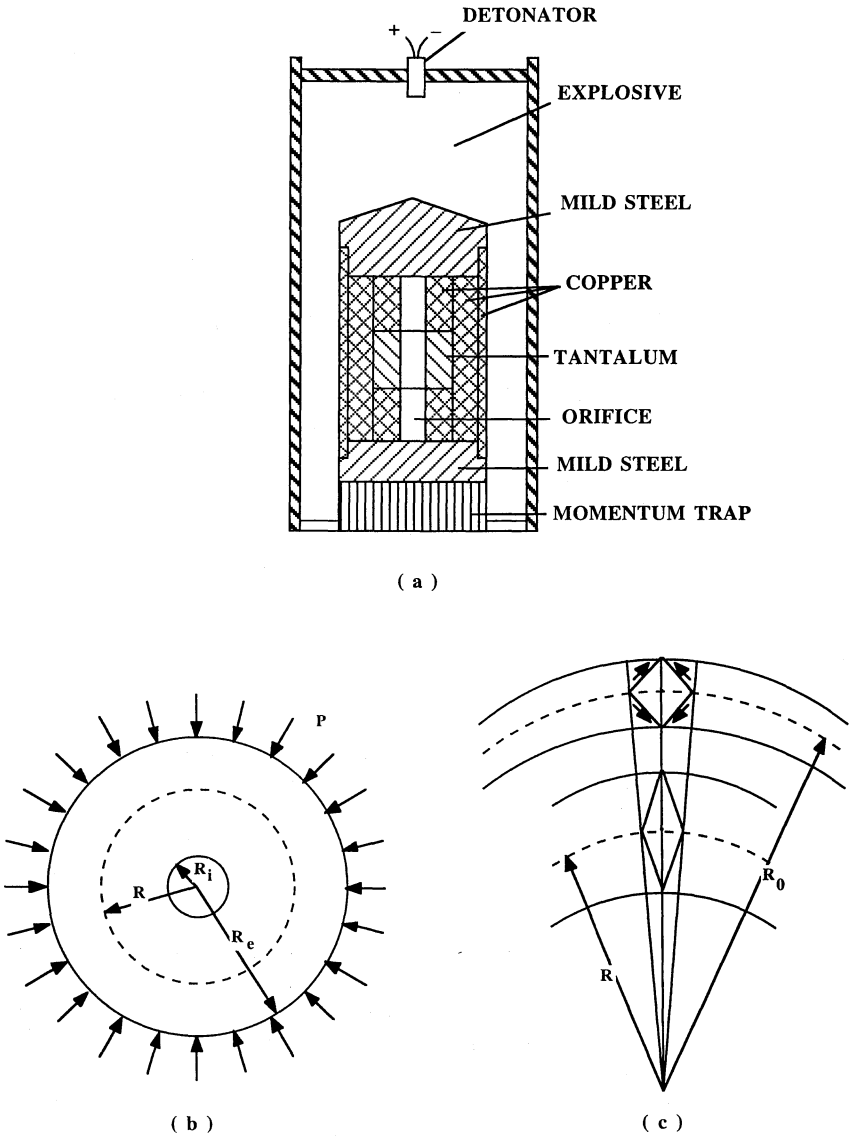

Fig. 1. Thick-walled cylinder method: (a) overall view of experimental configuration; (b) cross-section of set-up with initial configuration; (c) pure shear distortion undergone by element during radial collapse.

and co-workers on recovered shaped-charge [3–5] and EFP [6,7] specimens. They observed a broad range of microstructural features such as: dislocation cells, subboundaries, and recrystallized grains. The thermomechanical environment experienced by shaped charges and EFPs can be simulated under controlled laboratory conditions in which the plastic strain and strain rate can be prescribed. The hat-shaped specimen, developed by Meyer and Manwaring [8], has been shown by Meyers et al. [9] and Andrade et al. [10] to be very useful in the establishment of the high-strain, high-strain-rate response of copper. This technique has recently been applied to tantalum [11]. The limitation of this technique is that the maximum effective strain that can be achieved is ~ 1. The primary microstructural changes observed were dynamic recovery and the onset of dynamic recrystallization within isolated regions, due to heterogeneous plastic flow. The calculated mean temperature was 800 K, insufficient for global dynamic recrystallization. The thick-walled cylinder method, developed by Nesterenko and coworkers [12–14], enables the generation of higher effective strains (~ 3) under controlled high strain-rate conditions. This report describes the application of this technique to tantalum, the microstructural changes observed, and correlates them with the local thermal excursion.

2. Experimental procedure

2.1. Material

Two types of tantalum (Cabot) were used in this research program:

(a) Plate (8 mm thick). This material was obtained from Cabot, Boyertown, PA, in circular-plate form (155 mm diameter). The plate was produced by press forging 30 cm high ingots into 10 cm slabs, which are then annealed. This is followed by cross-rolling to the final thickness with intermediate anneals. This tantalum contained a fairly high dislocation density in the as-received state, because no anneal was carried out after the last pass. The material did not have a uniform grain size; the heterogeneous microstructure was composed of regions with average grain sizes of 43 and 73 μm. The average microhardness values for these samples varied between 103–155 HV50. The yield stress in compression at a strain rate of 8×10^{-4} s^{-1} was 250 MPa. Further details about the texture and high-strain-rate properties can be found in Meyers et al. [11]. The tubes obtained from the plate were 8 mm in height, with inner and outer diameters of 11 and 17 mm, respectively.

(b) Tubes. Two tantalum tubes 70 mm in length and with inner diameters of 15.7 and 11 mm, respectively, and outer diameters of 19 and 16 mm, respectively, were obtained from Cabot, Boyertown, PA. These tubes were obtained from annealed rods. As a result, the microstructure was homogeneous with an average grain size of 60 μm. The average microhardness for these samples varied between 98 and 131 HV50. The mechanical properties as specified by Cabot are: tensile strength, 248 MPa; yield strength, 173 MPa; and elongation to failure, 45%.

The presence of interstitials is very important because strain aging is known to have significant effects on the mechanical properties, increasing the flow stress and work hardening in the 300–600°C temperature range. This is clearly demonstrated by, among others, Krashchenko and Statsenko [15], Shields et al. [16], and Strutt et al. [17]. The principal interstitial contents, in parts per million, for the two materials are: disks (C: 60; O: 70; N: 10; H: 4); tubes (C: 25; O: 60; N: < 10; H: < 5). The material for disks (initially, in shape of plate) has a slightly higher interstitial content than the tube. This level of intersititials is expected to play a role in the flow stress and work hardening in the 300–600°C temperature range.

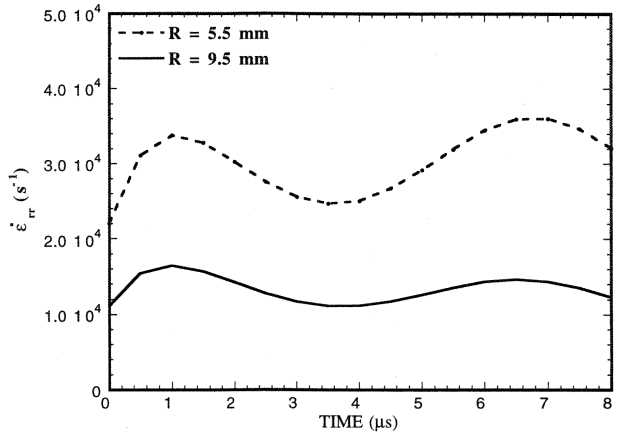

Fig. 2. Strain rates for inner and outer cylinder walls as a function of time after initiation walls as a function of time after initiation of collapse.

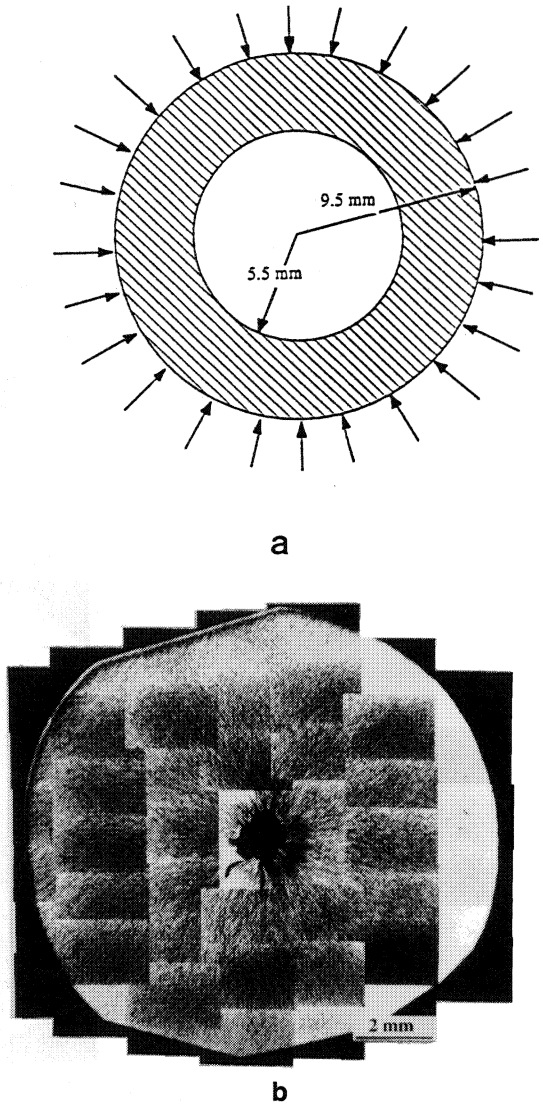

Fig. 3. (a) Initial and (b) final configurations for tantalum (disk).

2.2. The thick-walled cylinder method

The principal features of the thick-walled cylinder method are described first. The experimental configuration is shown schematically in Fig. 1(a). The inner wall of the tube is collapsed by the energy derived from the

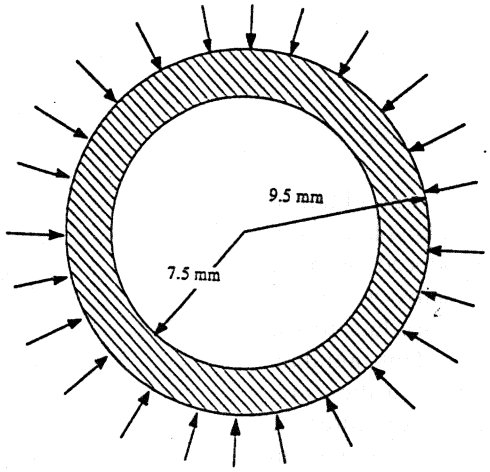

a

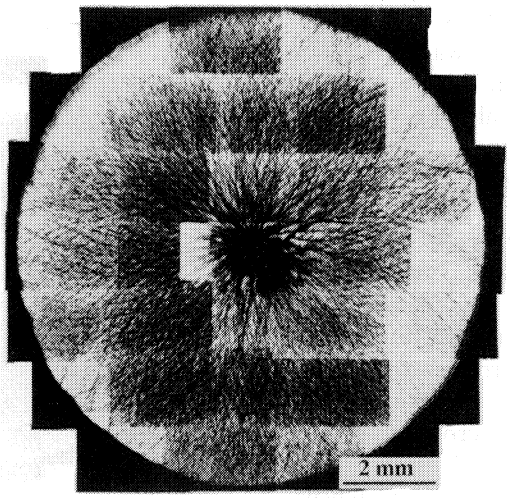

b

Fig. 4. (a) Initial; (b) final configurations for tantalum (tube); and (c) close up showing shear localization bands (arrows).

detonation of the low-detonation explosive charge, placed co-axially with the copper cylinder. The explosive is initiated at the top and the detonation wave proceeds downwards; thus, the inner wall of the tube does not collapse simultaneously. Nevertheless, the angle of collapse is very small, and plastic deformation can be assumed to occur in the plane perpendicular to the cylinder axis. An explosive with a detonation velocity of 4 km s^{-1} was used, and the system was calibrated by means of electromagnetic gages placed in the central orifice. This procedure is described by Nesterenko, Bondar, and Ershov [13]. Tantalum disks or tubes were incorporated into a copper thick-walled cylinder in such a fashion that they formed a portion of the internal wall. The insertion of the tantalum specimens did not appreciably change the plastic deformation parameters (strain and strain rate) because the Ta/Cu mass ratio is 0.2. Only the central portion of the setup was used, and wave propagation effects are essentially negligible because of the low detonation velocity of the explosive. Fig. 1(b) shows the cross-section of the system, with the external (R_e) and internal (R_i) radius of the Ta specimens. The final internal radius of Ta can be taken as zero.

In the case of disks, two were stacked up in the central portion of the assembly, for a total length of 16 mm. It was necessary to use disks because the material for EFPs has an initial thickness of 8 mm, insufficient for machining a tube. The tubular specimen was placed in the central portion, as marked. The state of strain is pure shear, as can be seen by the dimensional changes undergone by an initially square element, shown in Fig. 1(c). The strain rate as a function of time, calculated from the measured inner surface velocity [13,18], is

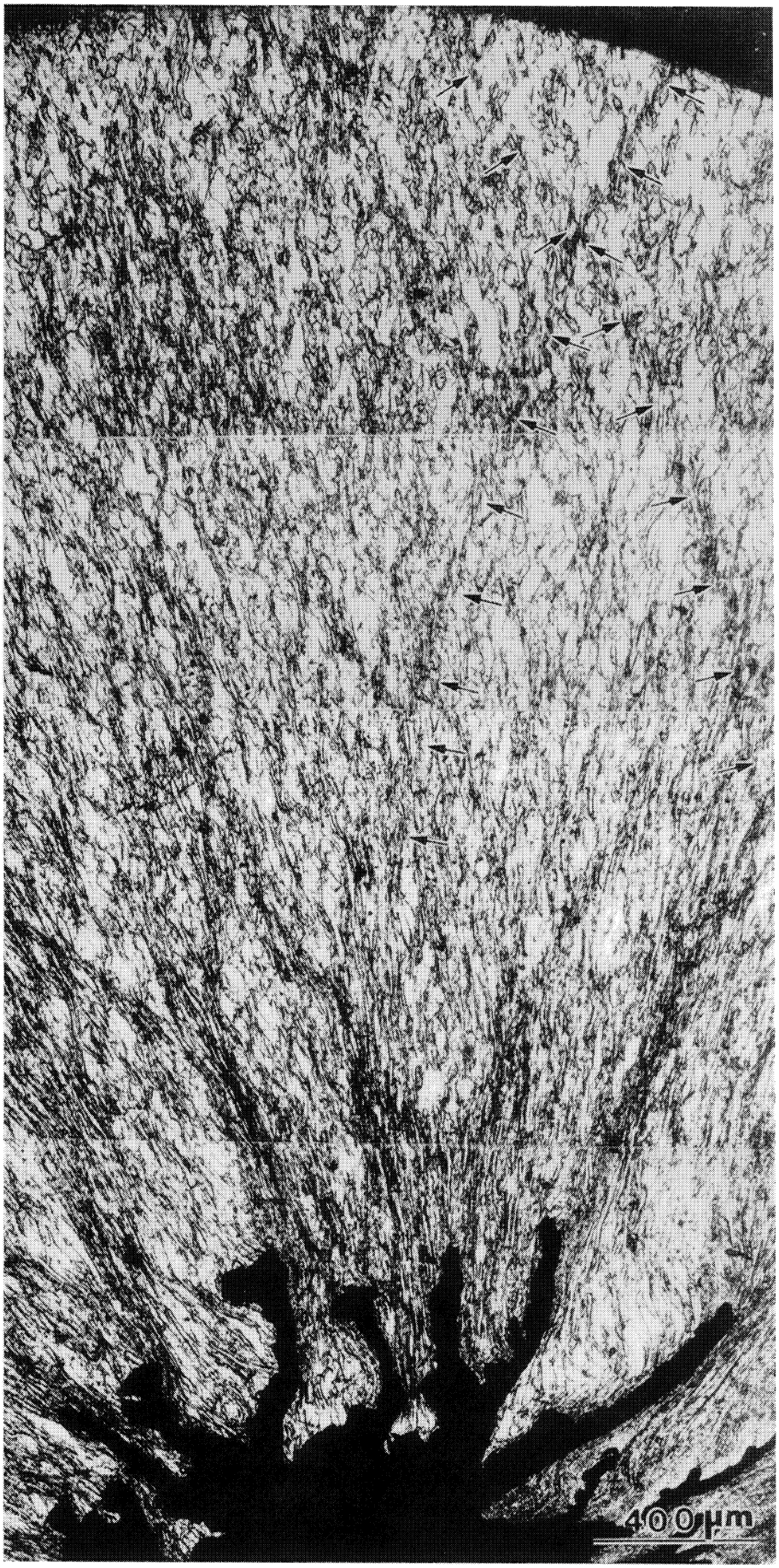

c

Fig. 4.

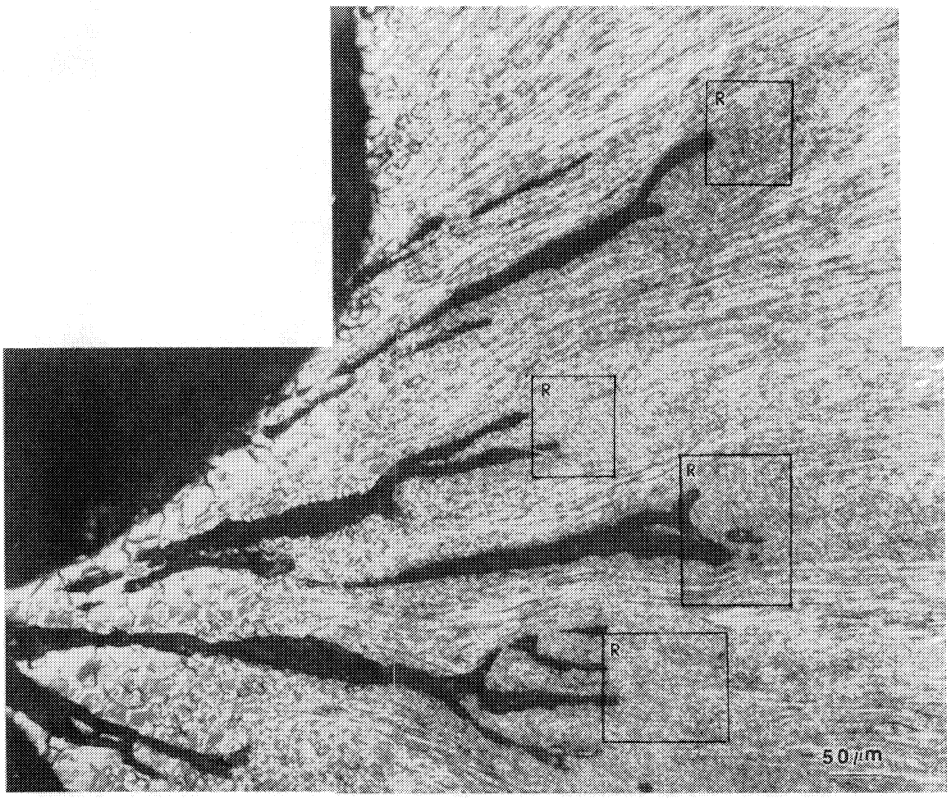

Fig. 5. Microstructure in vicinity of central hole.

shown in Fig. 2. As can be seen, the strain rate varies between 1 and 3.5×10^4 s^{-1} during the collapse process.

3. Results and discussion

3.1. Overall microstructural changes

The collapsed tantalum specimens are shown in Fig. 3 (disk and Fig. 4 (tube). Photomicrographs at two magnifications (Fig. 3) reveal the residual central orifice as well as a pattern of convergent plastic flow and radial cracks. The central orifice was not completely collapsed, and the residual radius is approximately 0.5 mm. This incomplete collapse is due to either jetting along the cylinder axis (due to non-simultaneity of cylinder collapse—see Section 2) or to insufficient energy for collapse. Nevertheless, over 90% of the process of collapse was successfully achieved. The residual central orifice is more regular for the tubular specimen, as is the pattern of cracks (see Fig. 4(b)). As can be seen in Fig. 4(c), these cracks propagate mainly in shear localized regions very near the central orifice. With increasing radius (i.e. decreasing strain), the shear bands become diffuse as shown by the arrows in Fig. 4(c). Upon closer examination, the region close to the central orifice reveals a broad variety of microstructural features. The initial grain sizes for the tantalum disk and tube are 43–73 μm [11] and 60 μm, respectively. Near the central orifice, regions with a well-annealed structure, with grain size of ~17 μm, can be seen for the tantalum disk (Fig. 5). This reduction in grain size (from 60 to 17 μm) is indicative of recrystallization, and requires a temperature and time window sufficient for this process. The recrystallized grain size decreases as a

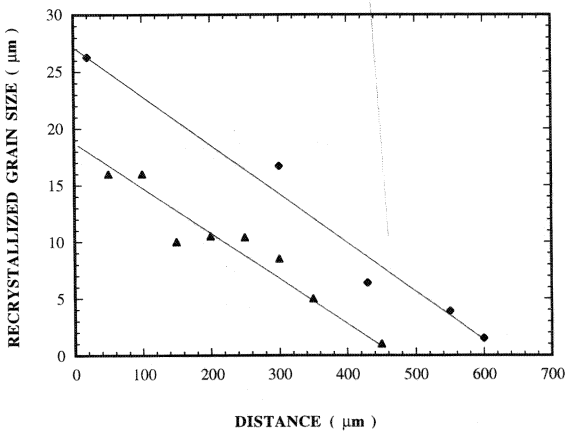

Fig. 6. Recrystallized grain size as a function of distance from the central axis in collapsed cylinder.

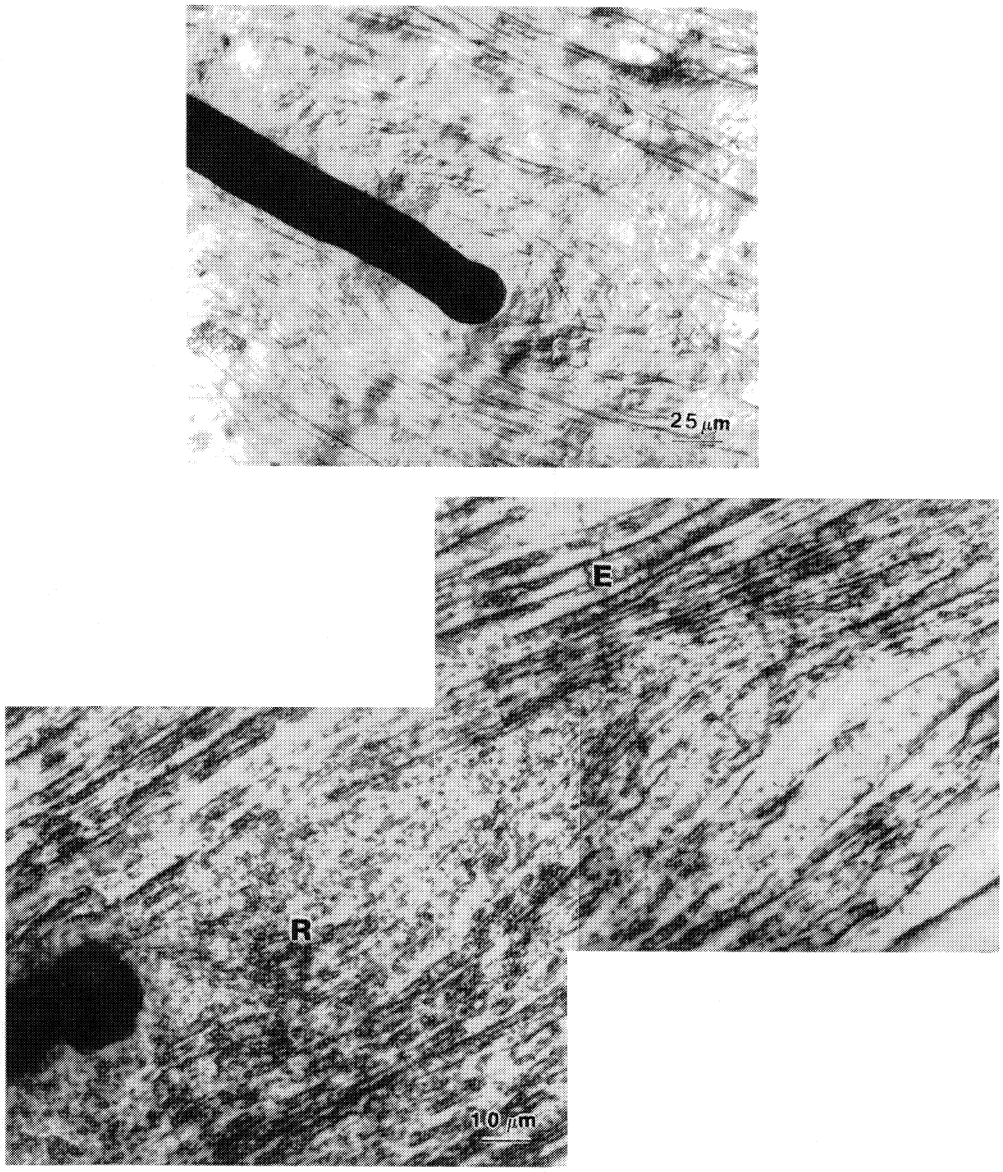

Fig. 7. Microstructural features of crack tips; note absence of alongated marks ahead of crack tips.

function of distance from the central orifice, until it cannot be resolved by optical metallography. Fig. 6 shows the measured recrystallized grain size as a function of distance. A straight-line approximation was used to represent this response. In Section 3.5, this recrystallized grain size is correlated with the thermal excursion undergone by the specimen. As the recrystallized grain size becomes too small to be resolved optically, two distinct areas appear: uniformly etched regions, marked *R* in Fig. 5 and indicated by rectangles; these regions are also shown in Fig. 7 as well as elongated features marked *E*. Fig. 7 shows the tips of two cracks. The material at the front of the cracks is more uniformly etched (*R*) whereas the material along the sides shows the elongated features (*E*). The crack tips show considerable blunting and a radius of ~ 10 μm. This is indicative of the ductile response of tantalum. The uniformly etched regions occur preferentially at the tips of the cracks and seem to be formed as poorly defined bands. The grain size was measured along two radii, and the variation falls within the band shown in Fig. 6. In Section 3.3 (transmission electron microscopy) these regions will be discussed further and clearly identified.

Microindentation hardness measurements were carried out radially and exhibited variations that are con-

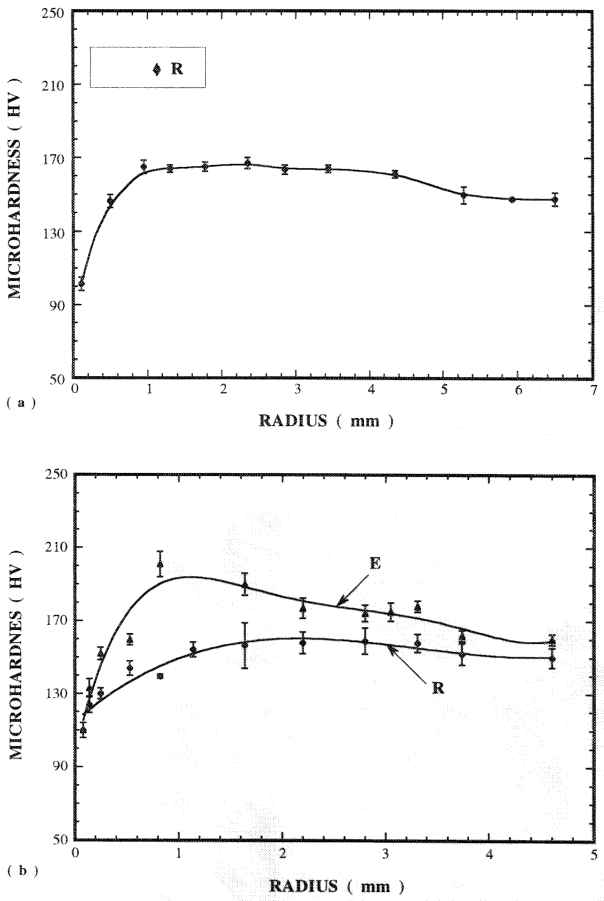

Fig. 8. Microindentation hardness as a function of distance from the central axis of collapsed cylinder: (a) disk specimens; (b) tube specimens.

sistent with the microstructural changes (see Fig. 8). The hardness increases gradually from the outer diameter toward the inside; this is a direct result of the increasing plastic strain. In the statically recrystallized region, close to central hole, there is a significant drop

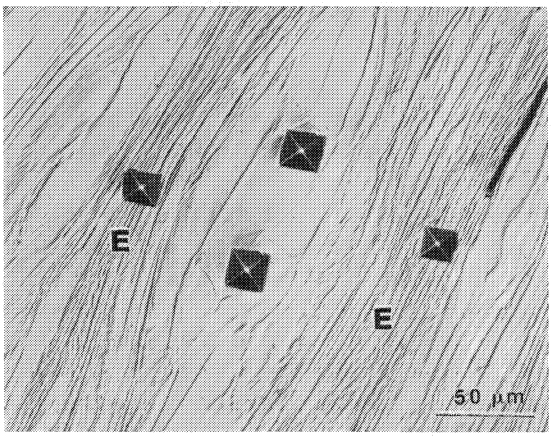

Fig. 9. Optical micrograph with microindentation hardness markings showing evidence for grain-scale localization.

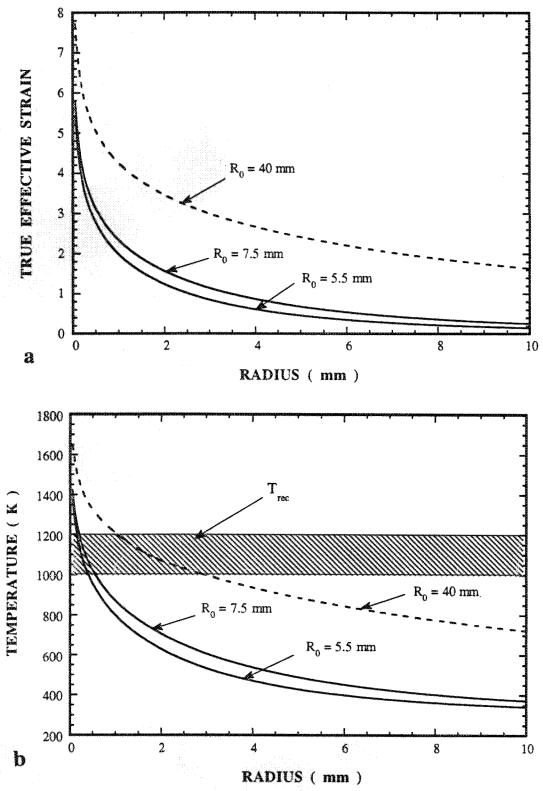

Fig. 10. (a) Effective strain and (b) temperature as a function of distance from central axis for total collapse of tantalum cylinder.

in hardness from the peak value, at HVN 170, to HVN 100. In the region adjoining this central hole, two levels of hardness appear: the hardness in the uniformly etched region (R) and the hardness in the elongated features (E) regions. It is possible to apply the Hall–Petch equation to hardness measurements. Meyers et al. [11] obtained a quasi-static (10^{-3} s^{-1}) flow stress of 300 MPa for the tantalum disk, consistent with the initial hardness of HVN 100, which corresponds to 980 MPa ($980/3 = 326$). The Hall–Petch parameters for tantalum are given by Armstrong [19] and Zerilli and Armstrong [20]:

$$\sigma = \sigma_0 + kd^{-1/2} \qquad 90 \le \sigma_0 \le 210 \text{ MPa}$$

$$9 \le k \le 19 \text{ MPa mm}^{1/2} \tag{1}$$

It should be considered that the initial condition of the tantalum is somewhat work-hardened and therefore the yield stress exceeds the predicted Hall-Petch value for 60 μm. Nevertheless it is possible to estimate a grain size for the areas R, exhibiting a value of HVN 200 (corresponding to 1960 MPa). The predicted grain size is, taking $k = 14$ MPa mm$^{1/2}$:

$$d = \left(\frac{k}{\frac{H}{3} - \sigma_0}\right)^2 \approx 0.1 \text{ μm} \tag{2}$$

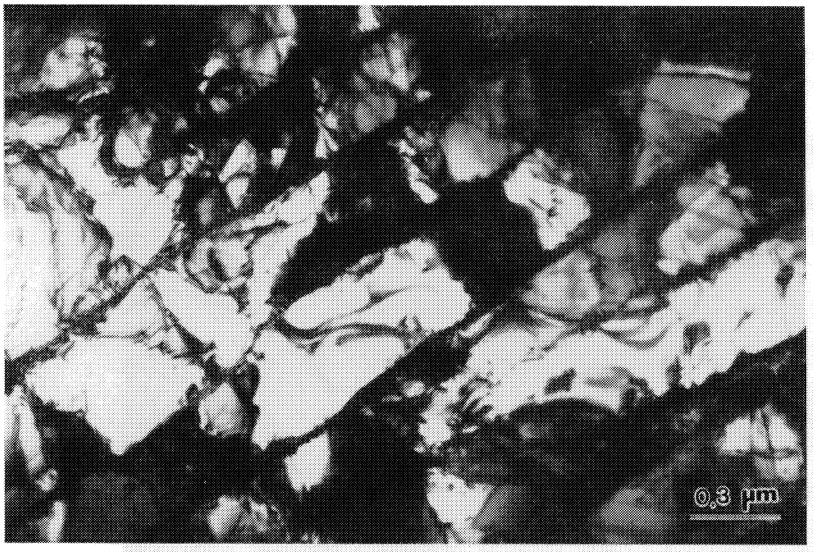

Fig. 11. Transmission electron micrograph of external region (effective strain ~ 1; $\Delta T \approx 200$ K).

H is the hardness expressed in SI units. Thus, assuming that the areas R are recrystallized (and this will be discussed further in Section 3.2) the prediction from microhardness measurements is for a grain size of ~ 0.1 μm. This will be discussed further in Section 3.2.

The peculiar feature of Ta behavior is that plastic deformation, being localized in separate regions (E), is accompanied by grains which are uniformly deformed with subsequent difference in microhardness (see Fig. 9). These regions of localized plastic deformation (E) are developed on the scale of separate elongated initial grains, that is determined as grain-scale localization.

3.2. Strain and temperature calculations

The strain in the cylinder can be computed as a function of the initial dimensional parameters [21]. For the specific dimensional parameters of the current experiments (internal radii of 5.5 and 7.5 mm for the disk and tubular specimens, respectively) the effective strains as a function of distance from the cylinder axis are given in Fig. 10. The effective strain is defined as, in cylindrical coordinates:

$$\epsilon_{\text{eff}} = \frac{\sqrt{2}}{3}\left[(\epsilon_{\text{rr}} - \epsilon_{\theta\theta})^2 + (\epsilon_{\text{rr}} - \epsilon_{\text{zz}})^2 + (\epsilon_{\theta\theta} - \epsilon_{\text{zz}})^2\right]^{1/2} \quad (3)$$

ϵ_{rr}, $\epsilon_{\theta\theta}$, and ϵ_{zz} are the radial, tangential, and longitudinal strains (principal strains). For the thick-walled geometry, $\epsilon_{\text{zz}} = 0$ and constancy of volume (negligible elastic strains) leads to: $\epsilon_{\theta\theta} = -\epsilon_{\text{rr}}$. The effective strain is therefore given by:

$$\epsilon_{\text{eff}} = \frac{2}{\sqrt{3}}\epsilon_{\text{rr}} \quad (4)$$

The true effective strains can reach very high values in the region adjoining the central axis. Whereas the maximum effective strain achieved in the localized zone using the hat-shaped specimen is 1.4 (corresponding to a shear strain of 5.5), values for the effective macroscopic strain can exceed this value considerably in the thick-walled cylinder, as shown in Fig. 10(a). The dashed line represents a hypothetical experiment for which the initial radius of the inner hole is 40 mm. Effective plastic strains in the range 0–10 can be achieved by this deformation method.

The application of a modified Johnson–Cook [22] constitutive equation with parameters provided by independent quasi-static and dynamic uniaxial compression tests is described by Meyers et al. [11]. The equation is expressed as:

$$\sigma = (\sigma_0 + B\epsilon^{\text{n}})[1 + C\log(\dot{\epsilon}/\dot{\epsilon}_0)]\,\text{e}^{-\lambda(T - T_{\text{r}})} \quad (5)$$

where σ_0 is the yield stress, B and n are work-hardening parameters, C is a strain-rate sensitivity parameter, ϵ_0 and T_{r} are reference strain rate and temperature, respectively, and λ is a thermal softening parameter. The temperature rise as a function of strain becomes (assuming 90% conversion of plastic work into heat):

$$T = T_{\text{r}} + \frac{1}{\lambda}\ln\left\{\text{e}^{\lambda(T_0 - T_{\text{r}})} + \left(\frac{0.9\lambda\epsilon}{\rho C_{\text{p}}}\right)[1 + C\log(\dot{\epsilon}/\dot{\epsilon}_0)]\left(\sigma_0 + \frac{B}{n+1}\epsilon^{\text{n}}\right)\right\} \quad (6)$$

The results are shown in Fig. 10(b). The calculation was conducted for a strain rate of $\sim 4 \times 10^4$ s^{-1}, which characterizes the strain rate of the inner wall of the cylinder (see Fig. 2).

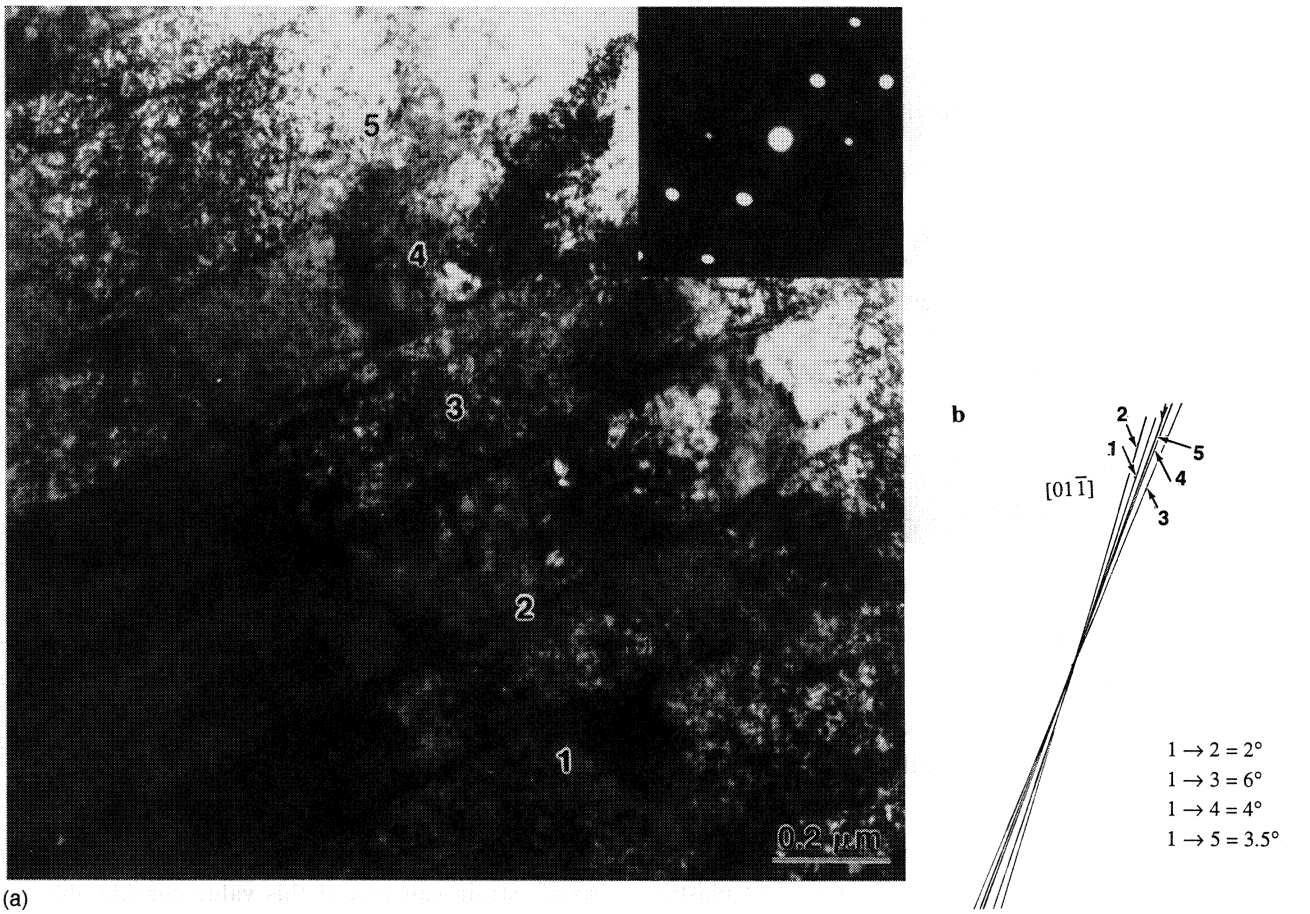

Fig. 12. (a) Transmission electron micrograph from region approximately 1.5 mm from central axis (effective strain: ~ 1.8; $\Delta T \approx 400$ K); diffraction patterns from sub-grain 4; (b) orientations of [1$\bar{1}$0] in five subgrains marked in (a).

3.3. Transmission electron microscopy

Transmission electron microscopy reveals the evolution of the microstructure as a function of plastic strain. As the central axis of the collapsed tubes are approached (increasing plastic strain), the microstructure evolves from isolated dislocations, to dislocation cells, to subgrains, and finally, to recrystallized grains. This sequence is entirely consistent with the results obtained earlier [10,11]. Fig. 11 shows the microstructure mid-way between the axis and the external surface at a distance of ~ 3 mm from the central axis. The dislocations organize themselves in walls, and the effective strain is ~ 1. The microstructure is very similar to the one observed by Andrade et al. [10] and Meyers et al. [11] for hat-shaped specimens.

Figs. 12–14 show the microstructure at a distance of ~ 1.5 mm from the internal wall. The high dislocation density leads to the formation of elongated cell walls. A set of several parallel cells separated by sub-boundaries is shown in Fig. 12(a); separate selected area electron diffraction patterns were made of the cells and the misorientations between adjacent cells are measured in Fig. 12(b). They are 2, 6, 4 and 3.5°. This is typical of a highly deformed structure ($\epsilon_{\text{eff}} \approx 2$). This microstructure is analogous to the one observed by Murr et al. [5] on recovered tantalum EFPs. These cells were also observed by Qiang et al. [2] and Wittman et al. [23]. The width of these cells is approximately 0.1–0.3 μm. Murr et al. [5] and Qiang et al. [2] measured misorientations varying between 3 and 8°. As the plastic deformation increases, the misorientation between adjacent cells increases and the cell walls become sharper. Fig. 13 shows well defined subgrains. The misorientation between two adjacent regions was measured and found to be higher than in Fig. 13: 10.6 and 5°. The gradual break-up of the elongated subgrains into micrograins is seen in Fig. 14. A similar break-up pattern was observed by Andrade et al. [10] for copper. The long subgrains break-up into grains having a more equiaxed structure with diameter equal to the width of the elongated sub-grains (~ 0.1 μm). The mechanism of rotation recrystallization, defined by Derby [24] corresponds, approximately, to this process. A micrograin, in the process of formation by a mechanism of migration (the second mechanism in Derby's classifica-

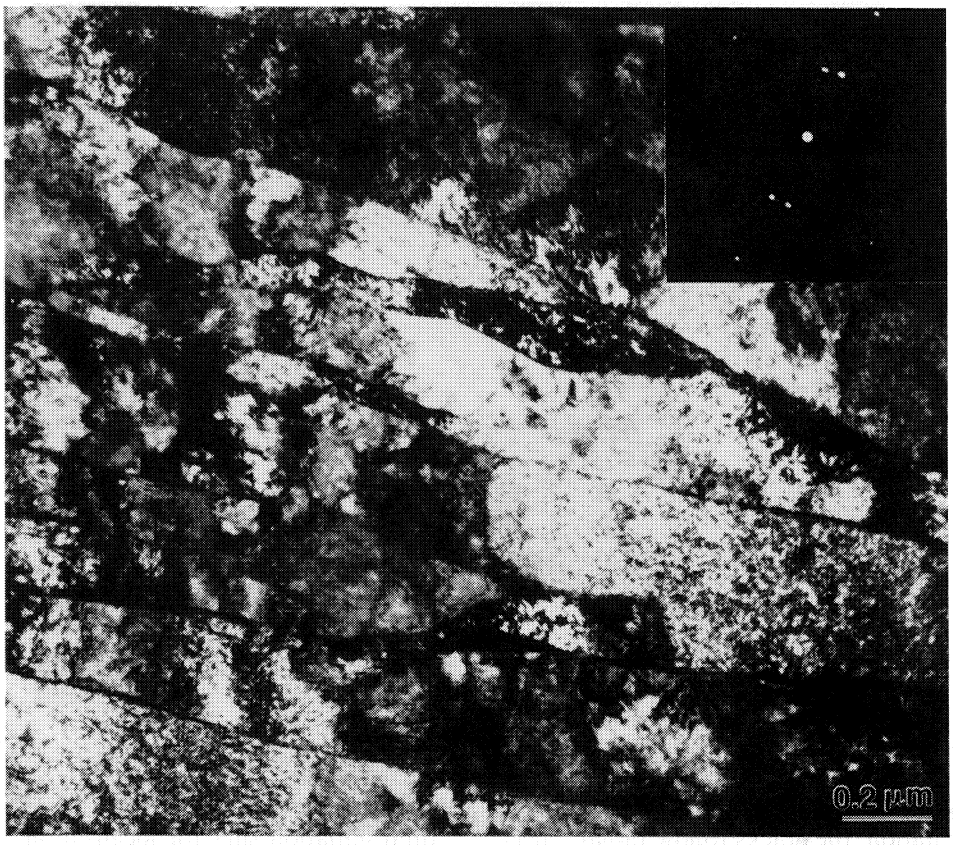

Fig. 13. Transmission electron micrograph of elongated sub-grains (~ 1.5 mm from central axis).

tion), can be seen in Fig. 14. It is indicated by arrow A. The arrow B indicates Moiré fringes from the boundaries between adjacent grains; these fringes suggest that the boundaries are sharp and well defined, and that they are no longer composed of dislocations. Thus, one may conclude as did Andrade et al. [10] that a combination of rotation and migration recrystallization are taking place. Whereas migration recrystallization requires significant diffusion, rotation recrystallization is primarily due to dislocation reorganization and does not require temperatures on the order of one-half the melting temperature. Rotation recrystallization is a characteristic feature of high strain deformation, as presented by Gil Sevillano et al. [25].

At even smaller distances from the central axis (~ 0.5 mm) the microstructure becomes decidedly broken down into micrograins with an aspect ratio of ~ 2–3 and a width of ~ 0.1 μm. The boundaries become clearly defined. The dark-field image of Fig. 15(a) is shown in Fig. 15(b) and the grain configuration is clear. The elongated subgrains are starting to partition into segments. This microstructure is not representative of the entire region, and grains with less deformation are juxtaposed with highly deformed grains. This is in accord with the optical micrographs of Figs. 5, 7 and 9, which show that plastic deformation is heterogeneous. Fig. 16 shows, through a sequence of dark-field images, how grain break-up leads to the recrystallized structure; corresponding grains in bright and dark-field images are marked by the 1-1, 2-2, and 3-3 pairs. The dihedral angles at the triple junctions indicate that the boundaries are large-angle. Fig. 16 is taken from an area marked *R* in Figs. 5 and 7.

3.4. Localization of plastic deformation

The formation of highly deformed bands juxtaposed with less deformed bands as the plastic strain is increased confirms earlier observations by Qiang et al. [2]. These bands provide thermal fluctuations which create the periodic array of softened regions that approximately have radial trajectories near the central orifice. Upon unloading, the residual tensile stresses produce opening along these bands, and the cracks serve as markers for them (Figs. 3 and 4). According to a preliminary analysis, after unloading, the residual tangential stress near the central orifice is tensile, becoming compressive at a radius of approximately 3.4 mm. This is an upper bound length estimate for mode *I* type cracks, and is consistent with the length of the cracks observed (see Fig. 3(b), 4(b) and (c)).

The following aspects are relevant:

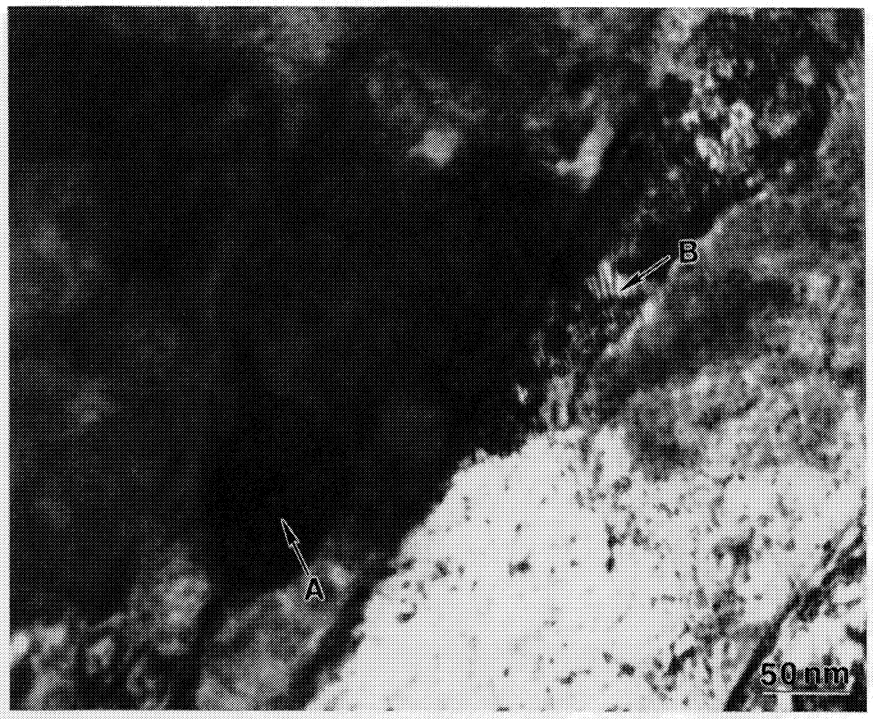

Fig. 14. Transmission electron micrograph from region approximately 1.5 mm from central axis showing break-up of elongated sub-grains.

(a) Crack length: it is approximately 0.5 mm.
(b) Crack orientation: the cracks follow radial trajectories and not spiral trajectories, such as in stainless steel and titanium (Nesterenko et al. [13]).

Vandermeer and Snyder [26] and Mitchell and Spitzig [27] studied the mechanical response of monocrystalline Ta and found profound differences in work hardening. These differences, in conjunction with texture softening, can lead to grain-scale localization. For instance, whereas the microhardness values of three monocrystals ((111); (112); (001)) were nearly equal, after 80% reduction in thickness the hardnesses were [26]:

HVN (111): 200
HVN (112): 150
HVN (001): 130

This is in line with the results of Mitchell and Spitzig [27]. An additional effect is texture softening, that becomes operative through plastic deformation due to the rotation of the grains towards orientations with larger Schmid factors. Asaro [28] showed that localization of plastic deformation can occur for crystals undergoing multiple shear with positive work hardening. Pierce et al. [29] applied this approach to strain-rate dependent metals and Asaro and Needleman [30] and Harren and Asaro [31] extended the treatment to polycrystals, using large-scale computations to predict shear localization in work-hardening materials. Gil Sevillano et al. [25] discuss the heterogeneity of plastic deformation at high strains, and Meyers et al. [32] included textural softening in their classification of microstructural initiation sites for localization.

The material is under a triaxial compression during the collapse of the cylinder and individual grains undergo very large extensions due to the pure shear imparted to them (see Fig. 1(c)). The length–width (aspect) ratio at a distance of 1 mm from the central axis ($\epsilon_{\text{eff}} = 1.8$; Fig. 10(a)) is 36/1. Under the action of the compressive stresses $\sigma_{\theta\theta}$, the 'softer' grains will deform more, and this can lead to much more pronounced grain distortions. As the internal radius of the cylinder is approached the strain rises to even higher ratios. For $\epsilon_{\text{eff}} = 3$, the aspect ratio is 400 and the length of an initially equiaxed grain of 30 μm is equal to 0.6 mm. Thus, grain-scale inhomogeneities of plastic deformation (texture softening and anisotropy of plastic flow) are thought to be the leading cause for localization of plastic deformation.

For tantalum, which is characterized by a constant work-hardening rate up to very large strains and high melting temperature, the traditional mechanism for the onset of shear localization (i.e. balance of thermal softening and work-hardening) can be less important than the texture softening mechanism. The texture softening mechanism naturally results in the diffuse shear bands because it requires the rotation of adjacent grains. The tubes produced from rods were more prone to forming diffuse shear bands.

It is worthwhile to mention that the number of regions in the specimen shown in Fig. 4 in which shear

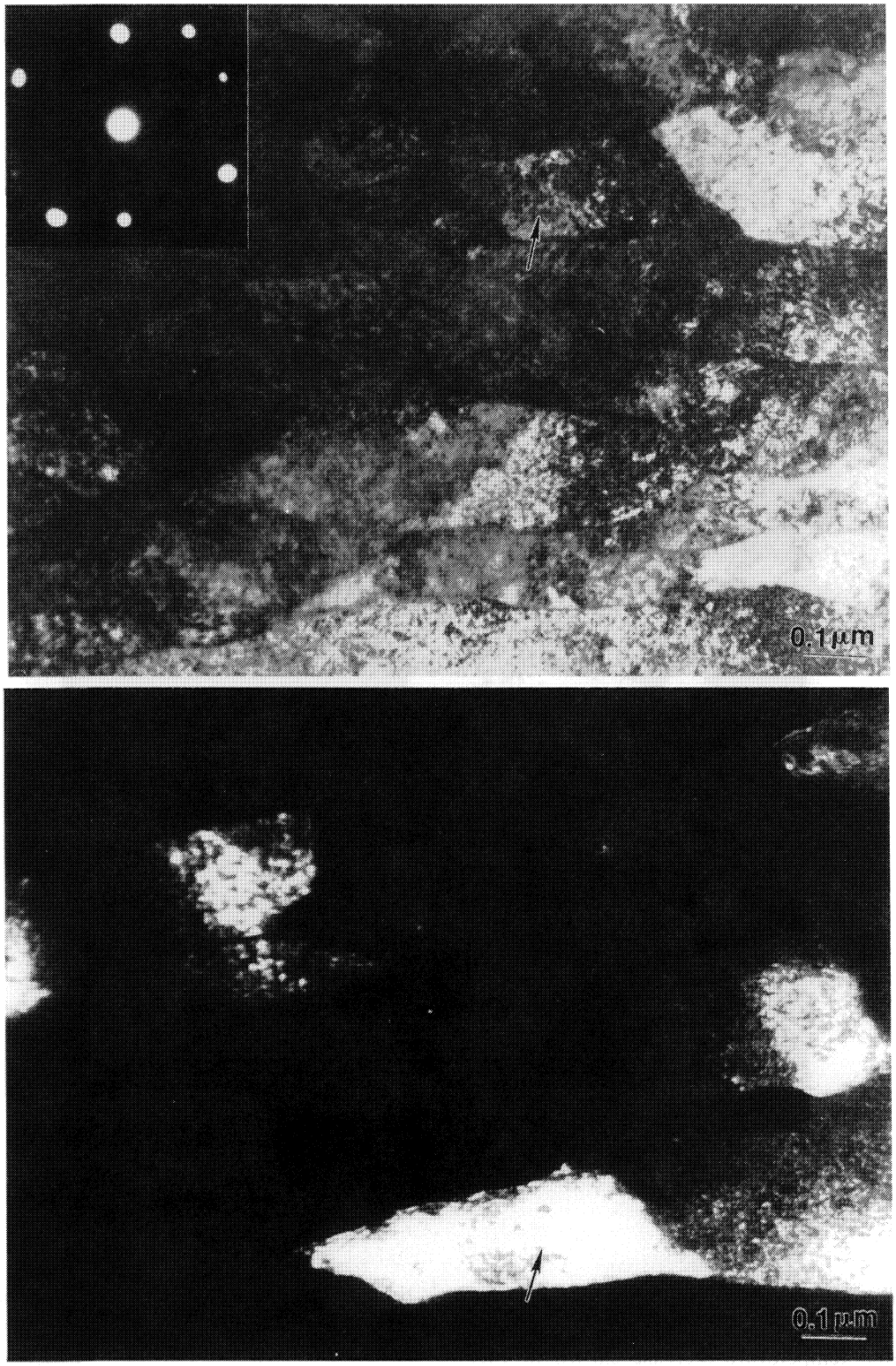

Fig. 15. Transmission electron micrograph of region close (< 0.5 mm) from central axis showing the break-up of the elongated subgrains: (a) bright field and diffraction pattern; (b) dark field.

deformation was localized is equal to 70. This is much higher than for titanium and stainless steel for the same overall macroscopic deformation. This demonstrates that the shear band spacing for tantalum is much smaller than for titanium and stainless steel.

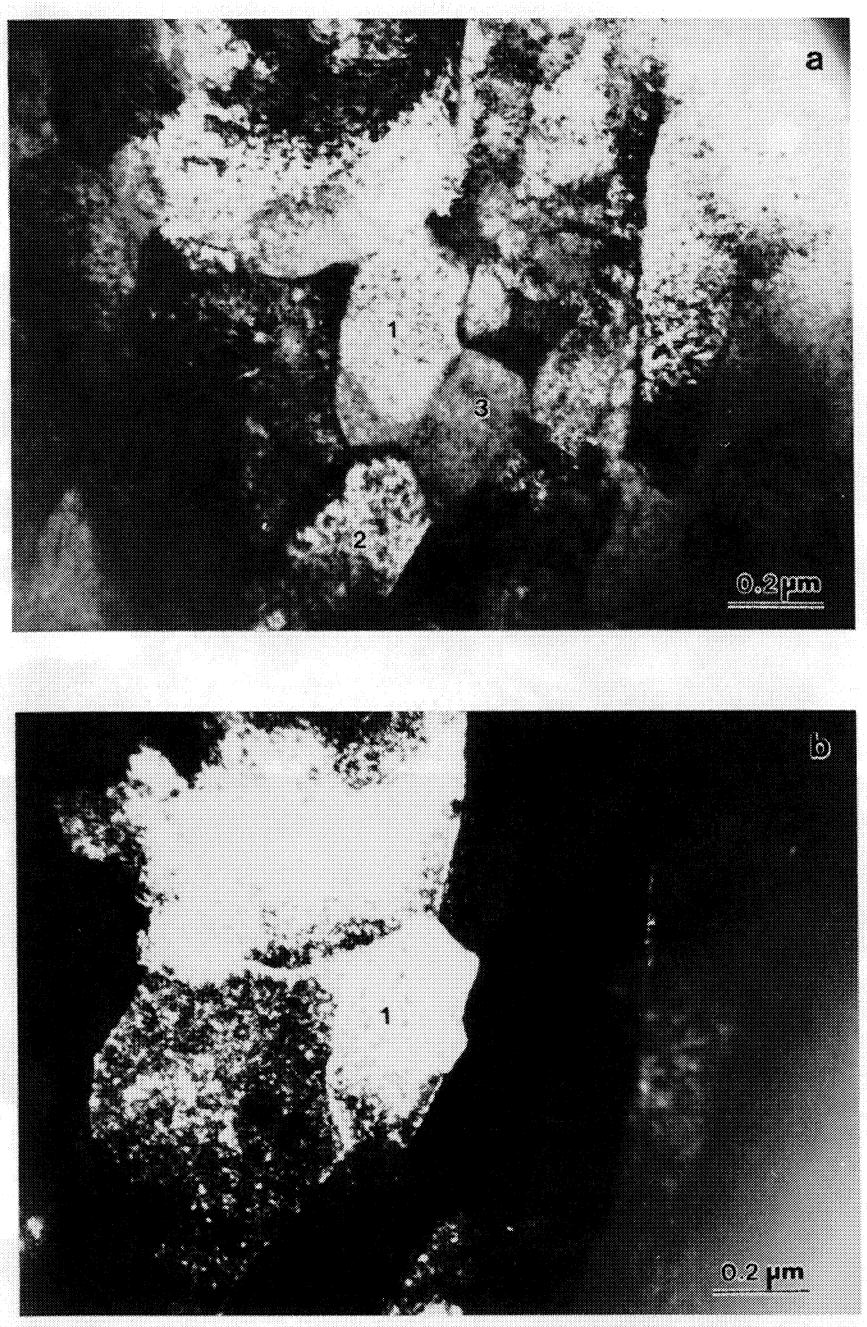

Fig. 16.

3.5. Recrystallization

The calculated temperature increase shown in Fig. 10(b) is suggestive of thermal recovery processes. The range of recrystallization temperatures is marked in Fig. 10(b). This range is estimated from data in the literature; Köck and Paschen [33] estimated the recrystallization range to be 1200–1500 K, whereas recent results by Beckenhauer et al. [34] yield a recrystallization temperature in high purity tantalum of 1000 K. Beckenhauer et al. [34] were able to obtain a lower recrystallization temperature by ultra-rapid heating (803 K s^{-1}) of the specimen, inhibiting recovery, a competing process. The conditions experienced by the dynamically deformed specimens resemble the ones simulated by Beckenhauer et al. [34] and this value is therefore taken as a lower bound for recrystallization. The results of the optical microscopy are entirely consistent with the temperature predictions of Fig. 10(b). A

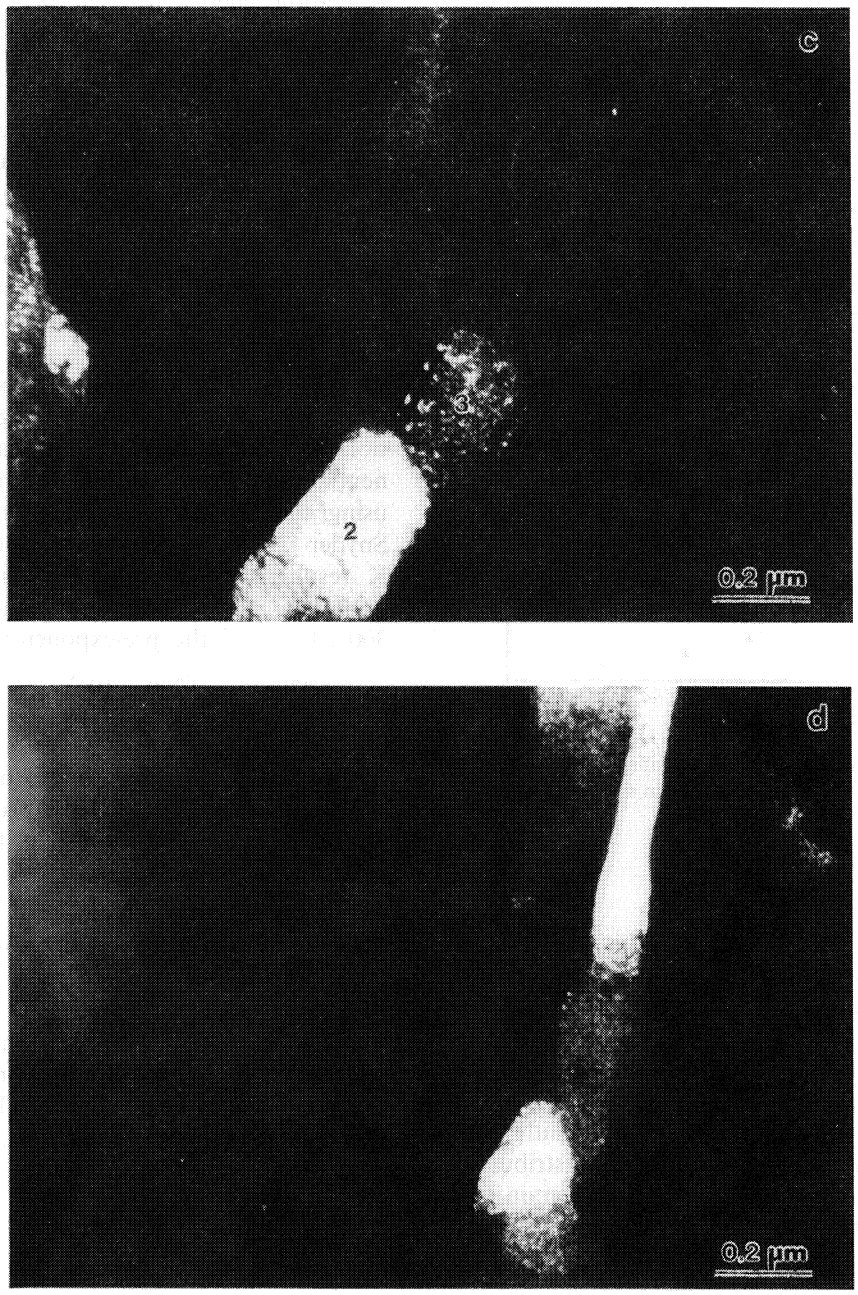

Fig. 16. (a) Bright-field and (b–d) dark-field images from a region < 0.5 mm from central axis showing recrystallized grains; notice grains 1-1, 2-2 and 3-3.

recrystallized layer with a width of ~ 0.5 mm is clearly seen, (Fig. 3(b)) and this corresponds to the lower hardness region in Fig. 8 and to the region in which the temperature approaches the recrystallization temperature in Fig. 10(b).

Two scales of recrystallization were observed: (a) recrystallization observed by optical microscopy, in the central region, with grain sizes ranging between 1–25 μm; and (b) recrystallization observed by transmission electron microscopy, localized in the regions ahead of the cracks, with grain sizes of approximately 0.1–0.3 μm. These will be discussed below.

3.5.1. Static recrystallization

Recrystallization can occur either concurrently or after deformation; it is called dynamic and static recrystallization, respectively. An estimate of the kinetics of static recrystallization can be obtained by calculations involving grain-boundary migration; static recrystallization occurs by a process of nucleation and growth of new grains. In order to establish this one can, to a first approximation, apply the simple grain growth equation (see Reed–Hill [35]):

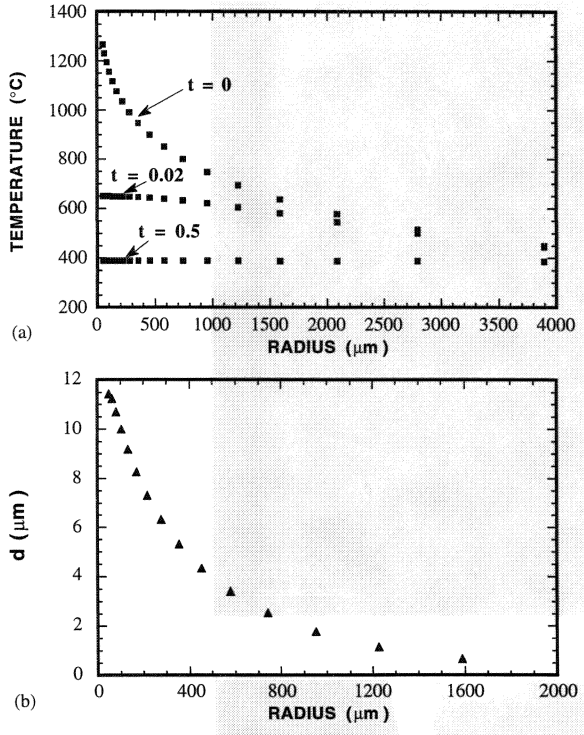

Fig. 17. (a) Calculated spatial temperature distribution for $t = 0$, 0.02, and 0.5 s; and (b) Calculated recrystallized grain size as a function of radius.

$$\Delta d = k_0 \Delta t^{1/n} \exp\left(-\frac{Q}{2RT(t)}\right) \tag{7}$$

where Δd is the change in the instantaneous grain size d, k_0 is a rate constant, Q is the activation energy for grain growth, Δt is the change in the time, and T is the absolute temperature. The time history of the temperature as a function of the distance from the central axis can be established from finite-difference heat transfer computations, assuming the distribution given in Fig. 10(b) at time $t = 0$. The initial grain size can be assumed to be zero. The activation energy for grain boundary migration, Q, can be taken as the activation energy for self-diffusion. This expression enables the calculation of the post-deformation grain sizes. The pre-exponential factor k_0 and the activation energy Q can be evaluated from experimental results reported in the literature. The exponent n varies between 2 and 10; it is 2 for ultrapure metals and growth is hindered by solute atoms, increasing n. The activation energy for diffusion, Q, was reported by Vandermeer and Snyder [26] to be equal to 394 kJ mol^{-1}. Krashchenko and Statsenko [15] report an activation energy for plastic deformation in the range of 0.47–0.54 T_m (where T_m is the melting point) of approximately 217 kJ mol^{-1}; this corresponds to the strain rate and temperature range for vacancy migration and diffusion along dislocations. The pre-exponential factor k_0 can be obtained from Eq. (7) by using the experimental result from Vandermeer and Snyder [26]: an annealing treatment of 7200 s at 1473 K resulted in a fully recrystallized structure with a grain size of 230 μm. Using an activation energy at 300 kJ mol^{-1} the pre-exponential factor is given by:

$$k_0 = \left(\frac{230^n}{7200}\right) \exp\left(\frac{300 \times 10^3}{2(1473)R}\right) \tag{8}$$

An estimate can be made of the recrystallized grain size as a function of distance from the central axis if the cooling rate is known. The final grain size is obtained by numerically integrating Eq. (7):

$$d = \left(\frac{230^n}{7200}\right) \exp\left(\frac{300 \times 10^3}{2(1473)R}\right) \sum_{i=1}^{N} \Delta t^{1/n} \exp\left(-\frac{Q}{2RT(t_i)}\right) \tag{9}$$

The temperature history as a function of radius was determined by solving the heat transfer problem using the finite-difference technique. The initial temperature distribution is given by Eq. (6). The radial strain is related to the final radius by:

$$\epsilon_{rr} = \ln\left(\frac{R_0}{R}\right) \tag{10}$$

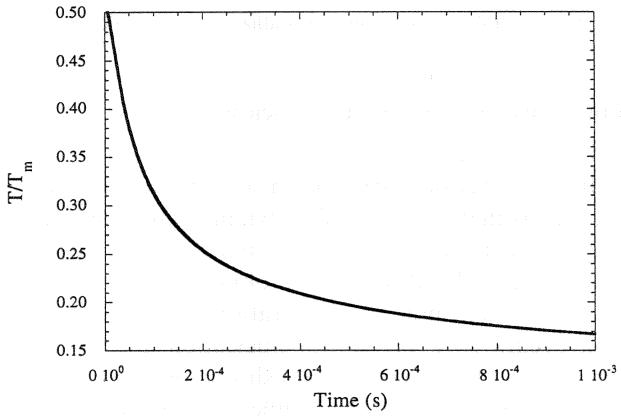

Fig. 18. Calculated cooling curve for a 100 μm wide shear band.

Fig. 17(a) shows the temperature as a function of radius (only up to 4 mm) for times $t = 0$, 0.02 and 0.5 s. The temperature is essentially uniform after 0.5 s. These values were incorporated into Eq. (9) to calculate the recrystallized grain size. The exponent n in Eq. (9) was varied to obtain results in reasonable agreement with experimental measurements. The use of $n = 8$ resulted in the grain-size profile shown in Fig. 17(b). The grain size decreases from 12 μm to less than 1μm for $0 < R < 1.2$ mm. This is consistent with the experimental values shown in Fig. 6. Thus, the recrystallized grains observed on the inner surface of the collapsed cylinder are probably due to static grain growth, and is most likely the result of a static recrystallization process.

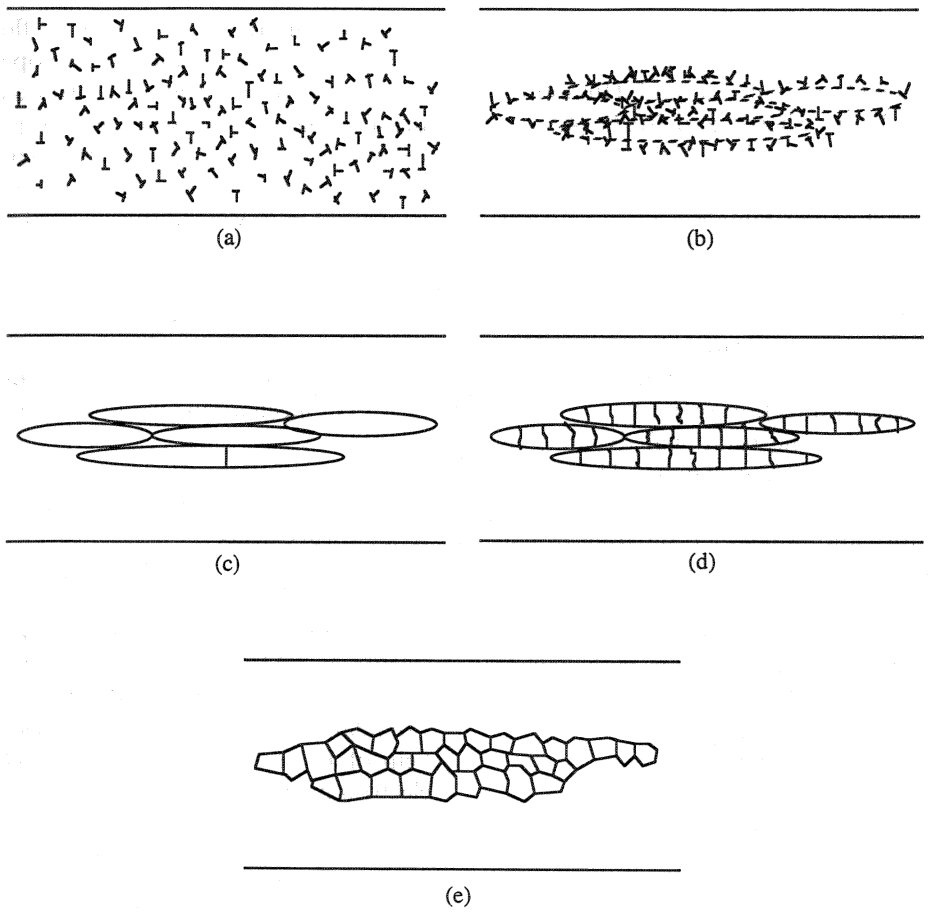

Fig. 19. Microstructural evolution in high-strain-rate deformation of tantalum: (a) uniform dislocation distribution; (b) elongated dislocation cells; (c) elongated subgrains; (d) subgrain break-up; (e) dynamically recrystallized grains.

3.5.2. Dynamic recrystallization

The regions marked *R* at the tips of the cracks (see Figs. 5 and 7) were revealed to be composed, through TEM observation (see Fig. 16), of small recrystallized grains with sizes in the range 0.1–0.3 μm. In these localized bands of plastic deformation, the temperature could reach the recrystallization range. However, the post-deformation cooling time is much shorter. It is possible to compute the temperature profile in a narrow band (100 μm width) initially at a temperature of equal to half the melting temperature. This band represents the tips of the cracks in Fig. 5. Fig. 18 shows the temperature history, calculated by finite-element analysis. The time is ~ 0.5 ms. It is possible to calculate the grain size obtained through a migrational recrystallization process by applying Eq. (9). A grain size of 8.6×10^{-4} μm is obtained. This is several orders of magnitude smaller than the grain size observed inside of the bands (0.1–0.3 μm).

The observation of substructural evolution suggests a different mechanism for recrystallization. Derby [24] classifies recrystallization mechanisms into rotational and migrational and attention will be focussed on the former one. Rotational recrystallization needs concurrent plastic deformation. It is well documented for geological materials such as quartz [36], halite [37], marble [38], sodium nitrate [39], and has recently been observed for copper by Andade et al. [10]; observations within shear bands in titanium are also suggestive of this mechanism [32,40]. Fig. 19 shows the primary features of the proposed mechanism. For convenience, it was divided into four stages. Random dislocation distribution (Stage 1) gives way to elongated dislocation cells (Stage 2) which become elongated subgrains (Stage 3) as deformation is increased. With further deformation, these subgrains breakup into micrograins which are approximately equiaxed (Stage 4) due to interfacial energy minimization. With continued deformation, these micrograins rotate. Takeuchi and Argon [41] suggested that the subgrain size resulting from high-temperature deformation was related to the applied stress by:

$$\frac{\sigma\delta}{\mu b} = K \tag{11}$$

where σ is the applied stress, δ is the subgrain size, μ is the elastic shear modulus, $\boldsymbol{b}$ is the Burgers vector magnitude, and $K \approx 10$ for metals. This is fairly similar to the expression obtained by Tungatt and Humphreys [39]. It is originally due to Sherby and Burke [42] and has its origin in low-temperature, high-stress creep. Derby [24] suggested that it could be applied to rotation recrystallization. For the tantalum in this investigation, the parameters are $\sigma = 500$ MPa, $\mu = 69$ GPa, and $\boldsymbol{b} = 0.2333$ nm. This yields a subgrain size of 0.3 μm, consistent with the observations. Thus, one may conclude that dynamic recrystallization by a rotational mechanism takes place in restricted regions of intense deformation (i.e. shear localization regions).

It is possible to analyze the rotational dynamic recrystallization from an energetic viewpoint. The overall energy due to random dislocation distribution (Stage 1), dislocation cell formation (Stage 2), subgrain formation (Stage 3), and micrograin formation (Stage 4) can be evaluated. This is described by Meyers et al. [43]. Calculations predict a critical dislocation density, misorientation, and cell sizes, in agreement with experimental observations.

4. Conclusions

(1) The collapse of a thick-walled cylinder was used to generate high plastic strains at high strain rates in tantalum. The plastic strain increases exponentially as the symmetry axis of the cylinder is approached; this technique propitiates controlled and reproducible plastic strains, at strain rates on the order of 4×10^4 s^{-1}.

(2) The microstructure was observed to evolve in the following sequence:

$0 < \epsilon_{ef} < 1$, dislocations and dislocation cells

$1 < \epsilon_{ef} < 2$, subgrains (dynamic recovery)

$2 < \epsilon_{ef} < 2.5$, subgrain break-up plus micrograins (dynamic recrystallization)

$\epsilon_{ef} > 2.5$, large equiaxed grains (static recrystallization)

This evolution is entirely consistent with the temperature rise predictions using a constitutive equation and Hopkinson bar experimental results obtained earlier by Meyers et al. [11]. The grain size of the statically recrystallized region is in agreement with calculations based on grain-growth kinetics coupled with the appropriate calculated cooling path.

(3) Profuse ductile cracks were observed (approximately 50) initiating at the internal surface of the central hole and propagating radially. These cracks are produced by residual tensie tangential stresses after the loading stages. The cracks propagate along bands of highly deformed material.

(4) The plastic deformation becomes heterogeneous after a critical strain with the formation of localization on the grain scale. This localization is due to texture softening and to the anisotropy of flow stress. The large aspect ratio (length–width) developed by the grains as they converge towards the central axis under the cylindrical collapse process generates plastic strains sufficient to induce large heterogeneities of flow. The localization follows the trajectory of flow of the grains (radial). Only very diffuse spiral shear bands were observed which follow the maximal macroscopic shear planes. The resulting temperature fluctuations generate radial paths of softened material.

(5) Dynamic recrystallization by a rotational mechanism occurs within regions of intense plastic deformation. A mechanism is proposed and qualitatively described.

Acknowledgements

This research was supported by the US Army Research Office, University Research Initiative Program (Contract DAAL-03-92-60108), by ARO Contract DAAH 04-93-G-0261, and by the National Science Foundation Institute for Mechanics and Materials. The help of Professor L.E. Murr and Dr C.-S. Niou with electron microscopy and extended discussions is greatly appreciated.

References

[1] M.J. Worswick, N. Qiang, P. Niessen and R.J. Pick, in M.A. Meyers, L.E. Murr and K.P. Staudhammer (eds.), *Shock-Wave and High-Strain-Rate Phenomena in Materials*, M. Dekker, New York, 1992, p 87.

[2] N. Qiang, P. Niessen and R.J. Pick, *Mater. Sci. Eng., A160* (1993) 49.

[3] A.C. Gurevitch, L.E. Murr, H.K. Shih, C.S. Niou, A.H. Advani, D. Manuel and L. Zernow, *Mater. Charact., 30* (1993) 201.

[4] H.K. Shih, C.-S. Niou, L.E. Murr and L. Zernow, *Scr. Metall. Mater., 29* (1993) 1291.

[5] L.E. Murr, C.-S. Niou and C. Feng, *Scr. Metall. Mater., 31* (1994) 297.

[6] L.E. Murr, H.K. Shih and C.-S. Niou, *Mater. Charact., 33* (1994) 65.

[7] L.E. Murr, C.-S. Niou, J.C. Sanchez and L. Zernow, *Metall. Mater., 32* (1995) 31.

[8] L.W. Meyer and S. Manwaring, in L.E. Murr, K.P. Staudhammer and M.A. Meyers (eds.), *Metallurgical Applications of Shock-Wave and High-Strain-Rate Phenomena*, Dekker, New York, 1986, p. 657.

[9] M.A. Meyers, L.W. Meyer, J. Beatty, U. Andrade, K.S. Vecchio and A.H. Chokshi, in M.A. Meyers, L.E. Murr and K.P. Staudhammer (eds.), *Shock-Wave and High-Strain-Rate Phenomena in Materials*, M. Dekker, New York, 1992, p 529.

[10] U.R. Andrade, M.A. Meyers, K.S. Vecchio and A.H. Chokshi, *Acta Metall. Mater., 42* (1994) 3183.

[11] M.A. Meyers, Y.-J. Chen, F.D.S. Marquis and D.S. Kim, *Metall. Mater. Trans., 26A* (1995) 2493.

[12] V.F. Nesterenko, A.N. Lazaridi and S.A. Pershin, *Fizika Goreniya i Vzryva., 25* (1989) 154.

[13] V.F. Nesterenko, M.P. Bondar and I.V. Ershov, in S.C. Schmidt, J.W. Shaner, G.A. Samara and M. Ross (eds.), *High-Pressure Science and Technology–1993*, AIP Press, New York, 1994, p. 1173.
[14] V.F. Nesterenko and M.P. Bondar, *DYMAT J.*, *1* (1994) 245.
[15] V.P. Krashchenko and V.E. Statsenko, *Strength of Matls.*, *13* (1981) 213.
[16] J.A. Shields, R. Gibala and T.E. Mitchell, *Metall. Trans. A*, *7A* (1976) 1111.
[17] A.J. Strutt, K.S. Vecchio, S.R. Bingert and G.T. Gray III, in *Proc. 1995 Int. Conf. on W and Refractory Metals, McLean, VA, MPIF.*
[18] V.F. Nesterenko, M.A. Meyers, H.C. Chen and J.C. LaSalvia, *Metall. Mater. Trans.*, *26A* (1995) 2511.
[19] R.W. Armstrong, in R.F. Bunshah (ed.), *Advances in Materials Research*, Vol. 5, Wiley Interscience, New York, 1971, p. 101.
[20] F.J. Zerilli and R.W. Armstrong, *J. Appl. Phys.*, *68* (1990) 1580.
[21] A. Mendelson, *Plasticity: Theory and Application*, Kreiger, Malabar, FL, 1968.
[22] G.R. Johnson and W.H. Cook, *Proc. 7th Intl. Symp. on Ballistics, The Hague, Netherlands, 1983*, p. 1.
[23] C.L. Wittman, R.K. Garrett, J.B. Clark and C.M. Lopatin, in M.A. Meyers, L.E. Murr and K.P. Staudhammer (eds.), *Shock-Wave and High-Strain-Rate Phenomena in Materials*, M. Dekker, New York, 1992, p. 925.
[24] B. Derby, *Acta Metall. Mater.*, *39* (1991) 955.
[25] J. Gil Sevillano, P. van Houtte and E. Aernoudt, *Prog. Mater. Sci.*, *25* (1981) 69.
[26] R. Vandermeer and W.B. Snyder Jr., *Metall. Trans. A*, *10A* (1979) 103.
[27] T.E. Mitchell and W.A. Spitzig, *Acta Metall.*, *13* (1965) 1169.
[28] R.J. Asaro, *Acta Metall.*, *27* (1979) 445.
[29] D. Pierce, R.J. Asaro and A. Needleman, *Acta Metall.*, *31* (1983) 1951.
[30] R.J. Asaro and A. Needleman, *Acta Metall.*, *33* (1958) 923.
[31] S.V. Harren and R.J. Asaro, *J. Mech. Phys. Solids*, *37* (1989) 191.
[32] M.A. Meyers, G. Subhash, B.K. Kad and L. Prasad, *Mech. Matls.*, *17* (1994) 175.
[33] W. Köck and P. Paschen, *J. Metals.*, *41* (10) (1989) 33.
[34] D. Beckenhauer, P. Niessen and P. Pick, *J. Mater. Sci.*, *12* (1993) 449.
[35] R.E. Reed-Hill, *Physical Metallurgy Principles*, 2nd edn., Van Nostrand, New York, 1973, p. 304.
[36] S. White, *Nature*, *244* (1973) 276.
[37] M. Guillope and J.P. Poirier, *J. Geoph. Res.*, *84* (1979) 5557.
[38] S.M. Schmid, M.S. Paterson and J.N. Boland, *Tectonophysics*, *65* (1980) 245.
[39] P.D. Tungatt and F.J. Humphrey, *Acta Metall.*, *32* (1984) 1625.
[40] M.A. Meyers and H.-r. Pak, *Acta Metall.*, *34* (1986) 2493.
[41] S. Takeuchi and A.S. Argon, *J. Mater. Sci.*, *11* (1976) 1547.
[42] O.D. Sherby and P.M. Burke, *Prog. Mater. Sci.*, *13* (1967) 325.
[43] M.A. Meyers, J.C. LaSalvia, V.F. Nesterenko, Y.J. Chen and B. Kad, *Proc. ReX 96, Monterey, CA, 1996.*

Instructions for Authors

SUBMISSION OF PAPERS

Manuscripts for the main part of the journal and for the Letters Section should be submitted as follows:

For authors in Europe

Editor-in-Chief
Professor Herbert Herman
Department of Materials Science and Engineering
State University of New York at Stony Brook
Long Island, NY 11794-2275
USA
Fax: +1 (516) 632 8052

or

Professor Gernot Kostorz
ETH Zurich
Institut für Angewandte Physik
CH-8093 Zurich
Switzerland
Fax: +41 (1633) 1105

For authors in Japan

Professor Masahiro Koiwa
Department of Materials Science and Engineering
Faculty of Engineering
Kyoto University
Yoshida-Honmachi, Sakyo-ku
Kyoto 606-01
Japan
Fax: +81 (75) 751 7844

For authors in North and South America and the rest of the world

Professor Herbert Herman
USA

or

Professor Carl C. Koch
North Carolina State University
Department of Materials Science and Engineering
233 Riddick Building
Yarbrough Drive
Raleigh, NC 27695-7907
USA
Fax: +1 (919) 515 7724

Manuscripts

Three copies should be submitted to the Editor, in double-spaced typing on pages of A4 size and with wide margins (Letters should not exceed 2000 words and a maximum of 5 figures). All tables and illustrations should bear a title or legend.
An *abstract* should accompany reviews, original papers and Letters. It should present (preferably in 100–150 words; 50 words or less for Letters) a brief and factual account of the contents and conclusions of the paper, and an indication of the relevance of new material.
References should be indicated by numerals in square brackets, introduced consecutively and appropriately in the text.

References must be listed on separate sheet(s) at the end of the paper. Every reference appearing in the text should be quoted in the reference list, and *vice versa*. When reference is made to a publication written by more than two authors it is preferable to give only the first author's name in the text followed by "*et al.*". However, in the list of references the names and initials of all authors must be given.
Three sets of figures should be submitted. One set of line drawings should be in a form suitable for reproduction, drawn in Indian ink on drawing or tracing paper (letter height, 3–5 mm). Alternatively, such illustrations may be supplied as high contrast, black-and-white glossy prints. Duplicate original micrographs should be provided wherever possible to facilitate the refereeing process. Magnifications should be indicated by a ruled scale bar on the micrograph. Captions to illustrations should be typed in sequence on a separate page.
All abbreviated terms must be defined when first used (both in the abstract and in the text) and authors must express all quantities in SI units, with other units in parentheses if desired.
Authors in Japan please note that information about how to have the English of your paper checked, corrected and improved (before submission) is available from:
Elsevier Science Japan
Higashi-Azabu 1-chome Building 4F
1-9-15 Higashi-Azabu
Minato-ku
Tokyo 106
Japan
Tel: +81-3-5561-5032; Fax: +81-3-5561-5045.

Further information

All questions arising after the acceptance of manuscripts, especially those relating to proofs, should be directed to:
Elsevier Editorial Services
Mayfield House
256 Banbury Road
Oxford OX2 7DH
UK
Tel. +44(0) 1865 314900; Fax. +44(0) 1865 314990.

Submission of electronic text

The final text may be submitted on a 3.5 in or 5.25 in diskette (in addition to a hard copy with original figures). Double density (DD) or high density (HD) diskettes are acceptable, but must be formatted to their capacity before the files are copied on to them. The main text, list of references, tables and figure legends should be stored in separate text files with clearly identifiable file names. The format of these files depends on the word processor used. WordPerfect 5.1 is the most preferable but for other formats please refer to the Instructions to Authors booklet. It is *essential* that the name and version of the wordprocessing program, type of computer on which the text was prepared, and format of the text files are clearly indicated.
The final manuscript may contain last minute corrections which are not included in the electronic text but such corrections must be clearly marked on the hard copy.